



Particle-in-cell Simulations of Decaying Plasma Turbulence: Linear Instabilities versus Nonlinear Processes in 3D and 2.5D Approximations

S. Peter Gary^{1,6} , Riddhi Bandyopadhyay^{2,6} , Ramiz A. Qudsi³ , William H. Matthaeus^{3,4} , Bennett A. Maruca^{3,4} ,
Tulasi N. Parashar⁵ , and Vadim Roytershteyn¹

¹ Space Science Institute, Boulder, CO, USA

² Department of Astrophysical Sciences, Princeton University, Princeton, NJ, USA

³ Department of Physics and Astronomy, University of Delaware, Newark, DE, USA

⁴ Bartol Research Institute, Newark, DE, USA

⁵ School of Chemistry and Physical Science, Victoria University of Wellington, 6012, New Zealand

Received 2020 June 23; revised 2020 August 18; accepted 2020 August 20; published 2020 October 6

Abstract

Particle-in-cell (PIC) simulations are used to examine the decay of strongly intermittent Alfvénic turbulence in a collisionless, homogeneous, and magnetized plasma. Results from three computational models are compared in simulations with similar plasma parameters and dimensions of approximately $100 d_i$, where d_i is the ion inertial length. Each model utilizes three-dimensional velocities, but spatial variations differ: the 2.5D perpendicular PIC model uses two-dimensional spatial variations with the background magnetic field \mathbf{B}_0 perpendicular to the simulation plane, the 2.5D parallel PIC model uses two-dimensional spatial variations with \mathbf{B}_0 in the simulation plane, and the 3D model includes spatial variations in full three-dimensional space. Results from the three models are compared using plots of the joint probability distribution functions (PDFs) of maximum local linear instability growth rates versus the maximum local nonlinear frequencies. All results agree with previous demonstrations that linear growth rates are generally slower than the nonlinear frequencies of the turbulence at $kd_i = 1.0$. However, it is the 3D PIC joint PDFs that most closely resemble joint PDFs recently observed in space plasmas because the 3D PDFs capture both the linear and nonlinear plasma processes, whereas the 2.5D parallel PIC runs do not represent the nonlinear turbulence processes and the 2.5D perpendicular PIC computations do not well represent the consequences of microinstabilities. These results suggest that 3D simulations are needed to properly capture important features of both microinstabilities and nonlinear turbulence.

Unified Astronomy Thesaurus concepts: [Interplanetary turbulence \(830\)](#); [Solar wind \(1534\)](#)

1. Introduction

The broadband, large-amplitude field fluctuations of collisionless, homogeneous, magnetized space plasma turbulence are observed to correspond to two distinct regimes, the long-wavelength “inertial range” typically described by fluid magnetohydrodynamic (MHD) models, and the shorter wavelength “kinetic range” that requires a velocity-space description. The typical MHD model of the inertial range cascade is that of a nonlinear transfer of field fluctuation energy being driven at the longest wavelengths down through the inertial range where dissipation is weak, followed by a transition to the steeper magnetic fluctuation spectra of the kinetic range where dissipation increases.

Representations of collisionless plasma turbulence are typically separated into two distinct categories. “Intermittent” turbulence is strongly nonlinear and fundamentally inhomogeneous ($\delta B \sim B_0$, where δB denotes the amplitude of a magnetic fluctuation and \mathbf{B}_0 represents the uniform background magnetic field; e.g., Matthaeus et al. 2015). Such turbulence is typically associated with the formation of sharp gradients and coherent structures such as current sheets, and is usually regarded as the primary constituent of the inertial range. Turbulence associated with short-wavelength microinstabilities is typically based upon the assumptions of a homogeneous plasma with relatively small amplitude fluctuations such that $\delta B \ll B_0$. The fluctuations of such turbulence satisfy dispersion properties derived

from linear kinetic theory (Gary 1993) such that the quasilinear premise is valid, where Klein et al. (2012) states this premise as the condition “that some characteristics of magnetized plasma turbulence can be usefully modeled as a collection of randomly phased linear wave modes.”

Both categories typically contribute to most space plasma turbulence observations; the wavenumber marking the difference between the inertial and kinetic ranges is of the order $kd_i \sim 1$, where d_i denotes the ion inertial length. A feature of the kinetic range is that the velocity-dependent plasma physics of this regime can, under sufficiently strong electron or ion anisotropies, lead to microinstability growth (Gary 1993); the resulting enhanced field fluctuations may scatter resonant charged particles and thereby act to dissipate this type of turbulence. But intermittent turbulence can also extend down to the shorter wavelengths of the kinetic range where wave-particle interactions can also dissipate this turbulence. Our consideration of turbulent dissipation here focuses on length scales at the small-scale end of the inertial range and the nearby scale lengths of the kinetic range. This transition regime is where the fastest Kolmogorov-like nonlinear effects should arise, as has been argued by Matthaeus et al. (2014). But there is a key difference between the results obtained by Matthaeus et al. (2014) and the consequences reported here. That difference is that the former nonlinear times are computed from the nonintermittent turbulence estimates of Kolmogorov (1941a, 1941b), which give a uniform estimation of nonlinear times, whereas the results presented here include intermittency

⁶ The research contributions to this work by S.P.G. and R.B., although distinct, were similar in magnitude.

effects as in Kolmogorov (1962) and therefore yield nonlinear times that are highly nonuniform.

Numerical studies of turbulence in collisionless, homogeneous, magnetized plasmas have been carried out using many different representations including single-fluid models (such as MHD), hybrid models in which electrons are represented as a fluid and ions are described as an ensemble of superparticles, and full particle-in-cell (PIC) models in which both electron and ion species are represented as superparticles satisfying Vlasov dynamics (Hockney & Eastwood 1981). We here address results from three PIC simulation models corresponding to three different dimensionalities for decaying plasma turbulence with the primary purpose of understanding the differences that arise from these models.

PIC simulations of collisionless plasmas follow the motion of a large number of superparticles, so that such calculations demand greater resources in terms of both computing time and computing grid resolution than do fluid or hybrid simulations with similar initial plasma parameters. So PIC simulations are likely to use unphysically small ion-to-electron mass ratios, relatively large values of v_A/c , and/or relatively short computational times. Another PIC approximation that has recently been used to reduce demands on computing resources is the use of the so-called “2.5D PIC” simulations in which the calculations follow the full three-dimensional velocity response of the superparticles, but allow plasma parameters to vary only in two spatial directions. The 2.5D approximation permits a larger number of particles and larger system sizes to be used for a given availability of resources. PIC simulations used to represent turbulence in collisionless, homogeneous, magnetized plasmas include four distinct models, which we label as follows:

1. *2.5D perpendicular PIC* simulations, which allow only two-dimensional spatial variations with \mathbf{B}_0 perpendicular to the simulation plane,
2. *2.5D oblique PIC* simulations, which also allow only two-dimensional spatial variations but with \mathbf{B}_0 neither strictly perpendicular nor strictly parallel to the simulation plane,
3. *2.5D parallel PIC* simulations, which again allow only two-dimensional spatial variations but with \mathbf{B}_0 in the simulation plane, and
4. *3D PIC* simulations with full three-dimensional spatial variations.

Recent 2.5D perpendicular PIC simulations of Alfvénic turbulence include Wu et al. (2013), Parashar et al. (2015a, 2018), Parashar & Matthaeus (2016), Matthaeus et al. (2016, 2020), Yang et al. (2017), Gonzalez et al. (2019), Roytershteyn et al. (2019), and Qudsi et al. (2020). Simulations of turbulence with 2.5D oblique PIC configurations include Wan et al. (2012), Karimabadi et al. (2013), and Yang et al. (2017). Alfvénic or magnetosonic-whistler turbulence has been the subject of 2.5D parallel PIC simulations by Gary & Saito (2003), Svidzinski et al. (2009), Camporeale & Burgess (2011), Saito et al. (2018), and Parashar & Gary (2019). Full 3D PIC simulations of Alfvénic or magnetosonic-whistler turbulence include Karimabadi et al. (2013), Roytershteyn et al. (2015), Parashar et al. (2015a), Wan et al. (2015, 2016), Hughes et al. (2017a, 2017b), Grošelj et al. (2018, 2019), Gary et al. (2016a, 2018), and Bandyopadhyay et al. (2020).

The physics of plasma turbulence with wavevector components in the plane of the background magnetic field is very different from the physics of such turbulence in a plane perpendicular to \mathbf{B}_0 . If there are no spatial variations in the parallel direction, then all wavevector components parallel to \mathbf{B}_0 are zero. Then the Landau resonances strictly apply only to fluctuations of zero frequency and the cyclotron resonances apply only to those waves with frequencies that exactly match the n th species cyclotron frequencies. So for 2.5D perpendicular PIC simulations both the Landau and cyclotron resonances are independent of particle velocities and the particles are constrained to fluid-like behavior. Although this may provide an appropriate description of long-wavelength turbulence, it fails to account for velocity-dependent wave-particle interactions, which may represent critical elements of turbulent dissipation at wavelengths of the order of or shorter than ion inertial lengths.

Analysis of results from PIC simulations of plasma turbulence often use probability distribution functions (PDFs) applied to various random variables of the computations. When such a variable is structureless and is due to an additive random process subject to the central limit theorem, its distribution is expected to be Gaussian; departures from the Gaussian condition often indicate new physics worthy of further study. In particular, as reviewed by Matthaeus et al. (2015), non-Gaussian PDFs of magnetic field component increments are indicators of intermittent plasma turbulence as has been demonstrated in both simulations (e.g., Wan et al. 2012, 2015; Karimabadi et al. 2013; Chang et al. 2014; Parashar et al. 2015a; Saito et al. 2018) and spacecraft observations (e.g., Parashar et al. 2018, 2020). A generalization of the single-variable PDF is the joint probability distribution that yields graphic displays of the correlations between two or more random variables. Examples of joint probability distributions in the analysis of space plasma turbulence observations include Bale et al. (2009), Maruca et al. (2011, 2012), Osman et al. (2012, 2013), Chen et al. (2016), Chasapis et al. (2018), and Woodham et al. (2019).

Bandyopadhyay et al. (2020) used joint PDFs to examine statistical relationships in kinetic range plasma turbulence in novel combinations, that is, between variables from both simulations and observations. Specifically, they used results from 3D PIC simulations, magnetosheath observations from MMS spacecraft, and solar wind measurements from the Wind spacecraft to examine statistical relationships between the local growth rate of electromagnetic proton temperature anisotropy instabilities as computed from collisionless plasma linear dispersion theory (Gary 1993) and the local nonlinear frequency ω_{nl} , which is defined by Equation (6) of Bandyopadhyay et al. (2020). Here we use this format to illustrate important differences among three models of decaying kinetic range Alfvénic turbulence, namely 2.5D perpendicular PIC, 2.5D parallel PIC, and 3D PIC.

2. Definitions and Simulation Parameters

We define the following: ω_{pj} is the j th species plasma frequency, Ω_j is the j th species cyclotron frequency, v_j is the j th species thermal speed, v_A is the Alfvén speed based on the ion mass, $\beta_j \equiv 8\pi n_j k_B T_{||j}/B_0^2$, the ion inertial length is $d_i = c/\omega_{pi}$, the computational time step is Δt and the simulation domain dimensions are $L_{||}$ and L_{\perp} where $||$ and \perp denote directions, respectively, parallel and perpendicular to \mathbf{B}_0 which is assumed

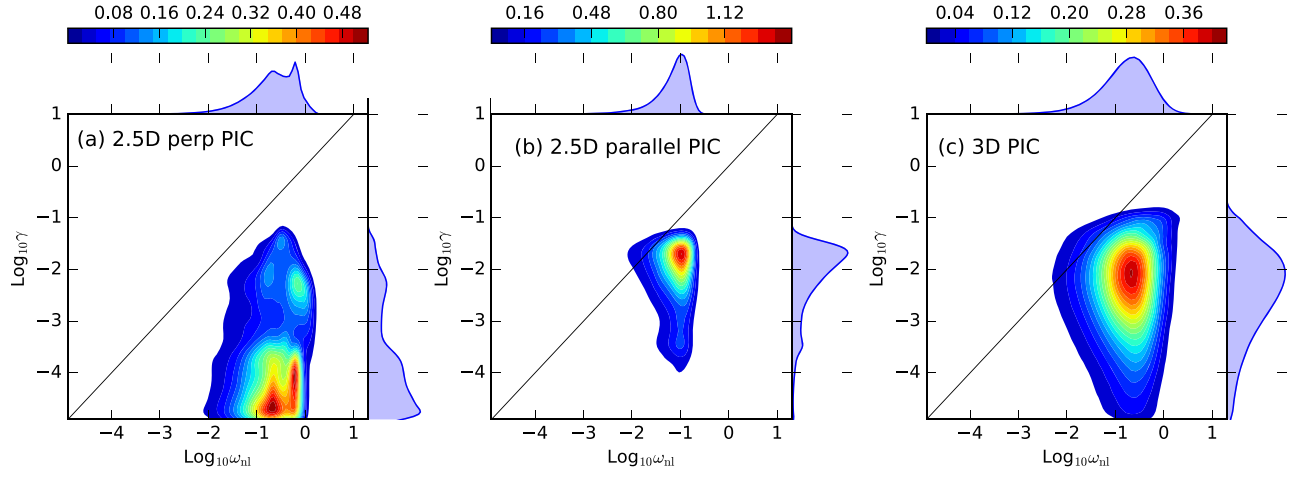


Figure 1. At $\omega_{\text{pet}} = 6000$ probability distribution functions (PDFs) for maximum instability growth rate γ from linear dispersion theory vs. the nonlinear frequency ω_{nl} for three simulations with similar initial conditions as described in the text: (a) the 2.5D perpendicular PIC Run 1, (b) the 2.5D parallel PIC Run 2, and (c) the 3D PIC Run 3. The joint PDF for Run 3 is computed by averaging over lags of $1 d_i$ in all three spatial directions. The straight line in each panel corresponds to $\omega_{\text{nl}} = \gamma$. The multicolored square panels contain the joint PDFs for each Run, and the light blue distributions on the boundaries of the square panels represent the 1D PDFs for the quantities as labeled.

to be uniform and constant. Subscripts e and i represent electrons and ions, respectively. The initial total fluctuating magnetic field energy density is denoted by $\varepsilon_o = \sum_k |\delta B_k|^2 / B_o^2$, which in other papers corresponds to $\delta B / B_o$.

To produce the PDFs, which illustrate the differences among the various PIC models, it is necessary to reduce the large body of data which is generated by the computations. The velocity distributions of space plasmas display a wide variety of nonthermal properties including ionic species, temperature anisotropies, and beam components (e.g., Dum et al. 1980; Gary et al. 2005, 2016b; Servidio et al. 2017). Here we follow the path of reduction sometimes used for such observations and assume the ion velocity distribution is a bi-Maxwellian (e.g., Kasper et al. 2002; Maruca et al. 2012) throughout each simulation. We further reduce the data by following Qudsi et al. (2020) and Bandyopadhyay et al. (2020) to use the resulting ion temperature anisotropies and $\beta_{\parallel i}$ values in a linear dispersion equation under the assumption of a collisionless, homogeneous, magnetized plasma (Gary 1993) to compute the associated maximum growth rates in each cell for each of the four electromagnetic ion anisotropy instabilities (i.e., Alfvén-cyclotron, ion mirror, ion parallel firehose, and ion oblique firehose). Under the assumption that the ion velocity distribution remains a bi-Maxwellian throughout each simulation, the local values of $T_{\perp i} / T_{\parallel i}$ and β_i across the simulation volume are used in conventional linear dispersion theory to compute the temporal growth rates for the various possible ion anisotropy instabilities. At late time in each simulation the maximum growth rate in each simulation cell is labeled γ , and is then used in the construction of the joint PDF as shown in Figure 1. Both Qudsi et al. (2020) and Bandyopadhyay et al. (2020) have emphasized that the strongly inhomogeneous character of the turbulence may invalidate the assumption of a homogeneous plasma; thus the values of γ should be regarded as qualitative, not quantitative, indicators of possible microinstability activity. In particular there are regions of a turbulent plasma in which the values of temperature anisotropy and plasma β may significantly depart from their volume averages.

A second reduced variable is the nonlinear frequency $\omega_{\text{nl}} = 2\pi / \tau_{\text{nl}}$, where $\tau_{\text{nl}}(\mathbf{r})$ is the local nonlinear timescale at

Table 1
Initial Values for the Plasma Parameters of Three Runs

	Run 1 2.5D Perpend- icular PIC	Run 2 2.5D Paral- lel PIC	Run 3 3D PIC
Simulation			
$\beta_e = \beta_i$	0.60	0.60	0.50
m_i / m_e	25	25	50
v_A / c	1/15	0.025	0.0707
$\omega_{\text{pe}} / \Omega_e$	3.0	8.0	2.0
Particles/cell/ species	3200	400	150
$\Omega_i \Delta t$	0.005	0.002	≈ 0.0008

point \mathbf{r} . Following Bandyopadhyay et al. (2020), we estimate this quantity as

$$\tau_{\text{nl}}(\mathbf{r}) \sim l / \delta b_l, \quad (1)$$

where δb_l is the longitudinal magnetic field increment in units of the Alfvén speed. Again following Bandyopadhyay et al. (2020), we focus on a spatial lag of $l = d_i$. Within a factor of 2π this is the characteristic scale for the spectral break between the inertial and kinetic ranges of the turbulent cascade as well as being the approximate wavenumber for maximum growth rate of the Alfvén-cyclotron, ion mirror, and ion firehose microinstabilities, so that we are indeed comparing the two processes at similar scale lengths. By analogy with the calculation of the maximum growth rate as discussed above, here also we compute the local values of the magnetic fluctuation components, and then do a statistical analysis of this data to construct the joint PDFs of Figure 1.

We compare results from three simulations of decaying Alfvénic plasma turbulence with initial plasma parameters as given in Table 1. Run 1 is a 2.5D perpendicular PIC run with $\mathbf{B}_o = B_o \mathbf{e}_z$ and the simulation plane in the x - and y -directions (this is the $\beta_i = \beta_e = 0.60$ simulation of Parashar et al. 2018). The simulation is carried out on a doubly periodic domain of size $L^2 = 4096^2$ cells, where $L_l = 149.6 d_i$, and $\Omega_i \Delta t = 0.005$. The initial conditions on the fluctuating

magnetic fields are a two-dimensional spectrum of Alfvénic fluctuations with $\varepsilon_o = 0.50$.

Run 2 is a 2.5D parallel PIC run with $\mathbf{B}_o = B_o \mathbf{e}_x$ and the simulation plane in the x - and y -directions (this is Run 3 from Parashar & Gary 2019). The simulation is carried out on a doubly periodic domain of size $L_\perp \times L_\parallel = 4043 \times 1000$ cells, where $L_\parallel = 149.6 d_i$, $L_\perp = 37.4 d_i$, and $\Omega_i \Delta t = 0.002$. The initial conditions on the fluctuating magnetic fields are a two-dimensional spectrum of Alfvénic fluctuations with $\varepsilon_o = 0.075$.

Run 3 is a full 3D PIC simulation with $\mathbf{B}_o = B_o \mathbf{e}_z$ as described in Roytershteyn et al. (2015). The simulation is carried out on a triply periodic domain of size $L^3 = 2048^3$ cells, where $L = 41 d_i$. The time step is $\Delta t \omega_{pe} \approx 0.08$. The initial conditions on the fluctuating magnetic fields are a fully three-dimensional spectrum of random Alfvénic fluctuations with $\varepsilon_o = 1.0$ as described by Roytershteyn et al. (2015).

3. Results

For each simulation Figure 1 presents, at the approximate time of maximum dissipation, one-dimensional PDFs for the maximum linear instability growth rate γ and the nonlinear frequency $\omega_{nl} = 1/\tau_{nl}$ as well as the joint PDF for these two variables. From the initial parameters chosen here, we draw the following conclusions:

- (1) Throughout most simulation domains

$$\gamma \ll \omega_{nl}. \quad (2)$$

This is consistent with previous linear instability theory and nonlinear PIC simulations (Matthaeus et al. 2014; Bandyopadhyay et al. 2020), as well as spacecraft observations of solar wind and magnetosheath plasmas (Bandyopadhyay et al. 2020).

- (2) The maximum value of the one-dimensional PDF for the Run 1 distribution is at a growth rate [$\text{Log}_{10}\gamma \approx -4.5$] much weaker than the corresponding maximum growth rates for Run 2 and Run 3 [$\text{Log}_{10}\gamma \approx -2$]. This is because the 2.5D perpendicular PIC simulation of Run 1 requires $k_\parallel = 0$ and therefore prevents growth of most kinetic instabilities, which are much more likely to arise in Run 2 and Run 3.
- (3) The maximum values of the nonlinear frequency distributions for all three runs are at roughly similar but not identical rates. The maximum value of the one-dimensional PDFs for both Run 1 and Run 3 peak near a value of $\text{Log}_{10}\omega_{nl} \approx -0.7$ to -0.8 , while the peak in Run 2 is around $\text{Log}_{10}\omega_{nl} \approx -1.0$. This is consistent with the calculation of ω_{nl} which is by definition taken at $kd_i = 1$, which is also the characteristic wavenumber of maximum growth for ion-driven electromagnetic instabilities such as the Alfvén-cyclotron anisotropy instability (Gary 1993, Section 7.2.2).
- (4) The one-dimensional PDFs of both γ and ω_{nl} are non-Gaussian for all three runs, indicating the respective processes are intermittent (e.g., Matthaeus et al. 2015), displaying elevated probabilities of extreme values.
- (5) The 3D PIC joint PDF of Run 3 shown in Figure 1(c) is similar in shape and scale to the joint PDF distribution obtained from MMS measurements shown as the central panel of Figure 4 in Bandyopadhyay et al. (2020). The other two panels of Figure 1 display rather different joint PDFs, suggesting that, under some circumstances, fully

3D PIC simulations may be necessary to accurately model spacecraft observations of turbulence.

- (6) Gary et al. (2000) derived

$$\nu_p \ll \gamma \quad (3)$$

where γ , as here, represents the maximum linear theory growth rate of the Alfvén cyclotron anisotropy instability but ν_p represents the maximum proton anisotropy scattering rate as determined from 2.5D parallel hybrid simulations of that instability in homogeneous collisionless plasmas. Equations (2) and (3) together imply that the forward cascade of Alfvénic turbulence from the inertial range to the kinetic range is much faster than either ion anisotropy instability growth or wave-particle scattering of the ions. And yet observations of different space plasma regimes (e.g., Gary et al. 2001; Kasper et al. 2002) as well as various kinetic simulations (e.g., Gary et al. 2000) show constraints that may be derived from ion anisotropy instability thresholds. This is the conundrum posed by Qudsi et al. (2020): “How can an inhomogeneous phenomenon such as turbulence be consistent with anisotropy constraints derived from linear theory of homogeneous plasmas?” It may be that, at least for the idealized case of a single bi-Maxwellian ion velocity distribution, the linear theory instability growth rate is independent of plasma density gradients. This hypothesis can be tested with a sequence of 3D PIC simulations of the Alfvén cyclotron anisotropy instability bearing successively steeper density gradients on the background plasma. But such a test is beyond the scope of this manuscript.

4. Conclusions

In the spirit of the Turbulent Dissipation Challenge (Parashar et al. 2015b) we have plotted results from three PIC simulations of the decay of strongly intermittent Alfvénic turbulence in a collisionless, homogeneous, magnetized plasma. We begin with similar plasma parameters but use three different spatial variation models, that is, 2.5D perpendicular PIC, 2.5D parallel PIC, and full 3D PIC, using joint PDFs to compare the late-time consequences of these models. All three models confirm previous demonstrations that linear growth rates of ion anisotropy microinstabilities are generally slower than the nonlinear frequencies of the turbulence. The PDF of the 2.5D parallel PIC simulation shows a greater similarity to the 3D PIC PDF at relatively large values of γ where microinstabilities should play a role, and the 2.5D perpendicular PIC PDF shows greater resemblance to the 3D PIC PDF at small values of γ where long-wavelength turbulence should dominate the physics.








Our results and Figure 4 of Bandyopadhyay et al. (2020) demonstrate that joint PDFs can be elegant and powerful tools for the study of the outstanding problem of linear instability theory versus nonlinear turbulence simulations. Such PDFs should also be helpful in the pursuit of the Turbulent Dissipation Challenge to demonstrate the comparative utility of other computational models such as 2.5D and 3D hybrid PIC (e.g., Parashar & Matthaeus 2016; Parashar et al. 2016), various gyrokinetic models (e.g., Navarro et al. 2016), and reduced kinetic models (e.g., Roytershteyn & Delzanno 2018). Due to the relatively small spatial extent and relatively short duration of the simulations, our results are likely to be

influenced by the initial conditions. Extending this analysis to a larger class of models and a range of plasma parameters would be a useful exercise. It would be particularly interesting to carry out a series of 2.5D oblique PIC simulations in which the angle between \mathbf{B}_0 and the simulation plane were varied to determine which angle provided the optimal representation of a full 3D PIC simulation. It would also be useful to increase the simulation box sizes to incorporate more consequences of the inertial range turbulence. It is also likely that larger systems would correspond to larger ion temperature anisotropies. We have not demonstrated that for larger systems the nonlinear rates would remain mostly faster than the linear instability rates as in the present study; however, we suspect that this ordering will remain valid. PDFs may also be used to directly illustrate the statistical properties of microinstabilities such as ion firehose modes (Matteini et al. 2011; Hellinger et al. 2019). But for each of these cases, we do not expect qualitative changes to arise; furthermore, such exercises would be beyond the purview of this work.

Note that PIC is not the only model used to represent the plasma turbulence cascade in the $kd_i \sim 1$ regime. For example, an alternate 3D velocity-space representation called the “Eulerian hybrid Vlasov-Maxwell” model has also been used for such studies (Cerri et al. 2018; Pezzi et al. 2019; differences between the two models and related questions are summarized in Cerri et al. 2019).

S.P.G. acknowledges support from NASA grants NNX17AH87G and NNX16AM98G (80NSSC19K0652) and NSF Award 2031024. W.H.M., R.B., and T.N.P. were partially supported by the MMS Theory and Modeling program under grant 80NSSC19K0565 at the University of Delaware. The research of R.B. and T.N.P. was carried out in part at the Department of Physics and Astronomy, University of Delaware, Newark, DE 19716. 3D PIC simulations were conducted as a part of the Blue Waters sustained-petascale computing project, supported by the National Science Foundation (NSF) awards OCI-0725070 and ACI-1238993 and the state of Illinois. Blue Waters allocation was provided by the NSF through PRAC award 1614664.

ORCID iDs

S. Peter Gary  <https://orcid.org/0000-0002-4655-2316>
 Riddhi Bandyopadhyay  <https://orcid.org/0000-0002-6962-0959>
 Ramiz A. Qudsi  <https://orcid.org/0000-0001-8358-0482>
 William H. Matthaeus  <https://orcid.org/0000-0001-7224-6024>
 Bennett A. Maruca  <https://orcid.org/0000-0002-2229-5618>
 Tulasi N. Parashar  <https://orcid.org/0000-0003-0602-8381>
 Vadim Roytershteyn  <https://orcid.org/0000-0003-1745-7587>

References

- Bale, S. D., Kasper, J. C., Howes, G. G., et al. 2009, *PhRvL*, **103**, 211101
 Bandyopadhyay, R., Qudsi, R. A., Matthaeus, W. H., et al. 2020, arXiv:2006.10316
 Camporeale, E., & Burgess, D. 2011, *ApJ*, **730**, 114, [Erratum: *ApJ*, 735, 6]
 Cerri, S. S., Grošelj, D., & Franci, L. 2019, *FrASS*, **6**, 64
 Cerri, S. S., Kunz, M. W., & Califano, F. 2018, *ApJL*, **856**, L13
 Chang, O., Gary, S. P., & Wang, J. 2014, *PhPI*, **21**, 052305
 Chasapis, A., Yang, Y., Matthaeus, W. H., et al. 2018, *ApJL*, **862**, 32
 Chen, C. H. K., Matteini, L., Schekochihin, A. A., et al. 2016, *ApJL*, **825**, L26
 Dum, C. T., Marsch, E., & Pilipp, W. 1980, *JPIPh*, **23**, 91
 Gary, S. P. 1993, *Theory of Space Plasma Microinstabilities* (New York: Cambridge Univ. Press)
 Gary, S. P., Hughes, R. S., & Wang, J. 2016a, *ApJ*, **816**, 102
 Gary, S. P., Jian, L. K., Broiles, T. W., et al. 2016b, *JGRA*, **121**, 30
 Gary, S. P., & Saito, S. 2003, *JGRA*, **108**, 1194
 Gary, S. P., Skoug, R. M., Steinberg, J. T., & Smith, C. W. 2001, *GeoRL*, **28**, 2759
 Gary, S. P., Smith, C. W., & Skoug, R. M. 2005, *JGRA*, **110**, A07108
 Gary, S. P., Yin, L., & Winske, D. 2000, *GeoRL*, **27**, 2457
 Gary, S. P., Zhao, Y., Hughes, R. S., Wang, J., & Parashar, T. N. 2018, *ApJ*, **859**, 110
 Gonzalez, C. A., Parashar, T. N., Gomez, D., Matthaeus, W. H., & Dmitruk, P. 2019, *PhPI*, **26**, 012306
 Grošelj, D., Mallet, A., Loureiro, N. F., & Jenko, F. 2018, *PhRvL*, **120**, 105101
 Grošelj, D. A., Chen, C. H. K., Mallet, A., et al. 2019, *PhRvX*, **9**, 031037
 Hellinger, P., Matteini, L., Landi, S., et al. 2019, *ApJ*, **883**, 178
 Hockney, R. W., & Eastwood, J. W. 1981, *Computer Simulation Using Particles* (Bristol: Institute of Physics Publishing)
 Hughes, R. S., Gary, S. P., & Wang, J. 2017a, *ApJL*, **835**, L15
 Hughes, R. S., Gary, S. P., Wang, J., & Parashar, T. N. 2017b, *ApJL*, **847**, L14
 Karimabadi, H., Roytershteyn, V., Wan, M., et al. 2013, *PhPI*, **20**, 012303
 Kasper, J. C., Lazarus, A. J., & Gary, S. P. 2002, *GeoRL*, **29**, 1839
 Klein, K. G., Howes, G. C., TenBarge, J. M., et al. 2012, *ApJ*, **755**, 159
 Kolmogorov, A. N. 1941a, *C. R. Acad. Sci. U.R.S.S.*, **32**, 16, [Reprinted in 1991, *RSPSA*, 434, 15]
 Kolmogorov, A. N. 1941b, *Dokl. Akad. Nauk SSSR*, **30**, 301, [Reprinted in 1991, *RSPSA*, 434, 9]
 Kolmogorov, A. N. 1962, *JFM*, **13**, 82
 Maruca, B. A., Kasper, J. C., & Bale, S. D. 2011, *PhRvL*, **107**, 201101
 Maruca, B. A., Kasper, J. C., & Gary, S. P. 2012, *ApJ*, **748**, 137
 Matteini, L., Hellinger, P., Landi, S., Travnicek, P. M., & Velli, M. 2011, *SSRv*, **172**, 373
 Matthaeus, W. H., Oughton, S., Osman, K. T., et al. 2014, *ApJ*, **790**, 155
 Matthaeus, W. H., Parashar, T. N., Wan, M., & Wu, P. 2016, *ApJL*, **827**, L7
 Matthaeus, W. H., Wan, M., Servidio, S., et al. 2015, *RSPTA*, **373**, 20140154
 Matthaeus, W. H., Yang, Y., Wan, M., Parashar, T. N., & Bandyopadhyay, R. 2020, *ApJ*, **891**, 101
 Navarro, A. B., Teaca, B., Told, D., et al. 2016, *PhRvL*, **117**, 245101
 Osman, K. T., Matthaeus, W. H., Hnat, B., & Chapman, S. C. 2012, *PhRvL*, **108**, 261103
 Osman, K. T., Matthaeus, W. H., Kiyani, K. H., Hnat, B., & Chapman, S. C. 2013, *PhRvL*, **111**, 201101
 Parashar, T. N., & Gary, S. P. 2019, *ApJ*, **882**, 29
 Parashar, T. N., Goldstein, M. L., Maruca, B. A., et al. 2020, *ApJS*, **246**, 58
 Parashar, T. N., & Matthaeus, W. H. 2016, *ApJ*, **832**, 57
 Parashar, T. N., Matthaeus, W. H., & Shay, M. A. 2018, *ApJL*, **864**, L21
 Parashar, T. N., Matthaeus, W. H., Shay, M. A., & Wan, M. 2015a, *ApJ*, **811**, 112
 Parashar, T. N., Oughton, S., Matthaeus, W. H., & Wan, M. 2016, *ApJ*, **824**, 44
 Parashar, T. N., Salem, C., Wicks, R. T., et al. 2015b, *JPIPh*, **81**, 905810513
 Pezzi, O., Yang, Y., Valentini, F., et al. 2019, *PhPI*, **26**, 072301
 Qudsi, R. A., Bandyopadhyay, R., Maruca, B., et al. 2020, *ApJ*, **895**, 83
 Roytershteyn, V., Boldrev, S., Delzanno, G. L., et al. 2019, *ApJ*, **870**, 103
 Roytershteyn, V., & Delzanno, G. L. 2018, *FrASS*, **5**, 27
 Roytershteyn, V., Karimabadi, H., & Roberts, A. 2015, *RSPTA*, **373**, 201140151
 Saito, S., Nariyuki, Y., & Umeda, T. 2018, *PhPI*, **25**, 122301
 Servidio, S., Chasapis, A., Matthaeus, W. H., et al. 2017, *PhRvL*, **119**, 205101
 Svidzinski, V. A., Li, H., Rose, H. A., Albright, B. J., & Bowers, K. J. 2009, *PhPI*, **16**, 122310
 Wan, M., Matthaeus, W. H., Karimabadi, H., et al. 2012, *PhRvL*, **109**, 195001
 Wan, M., Matthaeus, W. H., Roytershteyn, V., et al. 2015, *PhRvL*, **114**, 175002
 Wan, M., Matthaeus, W. H., Roytershteyn, V., et al. 2016, *PhPI*, **23**, 042307
 Woodham, L. D., Wicks, R. T., Verscharen, D., et al. 2019, *ApJL*, **884**, L53
 Wu, P., Wan, M., Matthaeus, W. H., Shay, M., & Swisdak, M. 2013, *PhRvL*, **111**, 121105
 Yang, Y., Matthaeus, W. H., Parashar, T. N., et al. 2017, *PhPI*, **24**, 072306